IOP Publishing Phys. Biol. 15 (2018) 056004 https://doi.org/10.1088/1478-3975/aac45b

Physical Biology

PAPER

RECEIVED
18 March 2018

REVISED
9 May 2018

ACCEPTED FOR PUBLICATION
14 May 2018

PUBLISHED
28 May 2018

Dynamic seesaw model for rapid signaling responses in eukaryotic chemotaxis

Shi Liang Feng[1,2], Lü Wen Zhou[1,2], Shou Qin Lü[2,3,4,5] and Yan Zhang[2,3,4,5]

[1] Institute of mechanical engineering and mechanics, Ningbo University, Ningbo 315211, People's Republic of China
[2] Center of Biomechanics and Bioengineering and Institute of Mechanics, Chinese Academy of Sciences, Beijing 100190, People's Republic of China
[3] Key Laboratory of Microgravity (National Microgravity Laboratory), Institute of Mechanics, Chinese Academy of Sciences, Beijing 100190, People's Republic of China
[4] Beijing Key Laboratory of Engineered Construction and Mechanobiology, Institute of Mechanics, Chinese Academy of Sciences, Beijing 100190, People's Republic of China
[5] School of Engineering Science, University of Chinese Academy of Sciences, Beijing 100049, People's Republic of China

E-mail: fengshiliang@nbu.edu.cn (S Feng) and zhangyan@imech.ac.cn (Y Zhang)

Keywords: polarization, signaling cascade, mathematical model, lattice–Boltzmann method

Supplementary material for this article is available online

Abstract

Directed movement of eukaryotic cells toward spatiotemporally varied chemotactic stimuli enables rapid intracellular signaling responses. While macroscopic cellular manifestation is shaped by balancing external stimuli strength with finite internal delays, the organizing principles of the underlying molecular mechanisms remain to be clarified. Here, we developed a novel modeling framework based on a simple seesaw mechanism to elucidate how cells repeatedly reverse polarity. As a key feature of the modeling, the bottom module of bidirectional molecular transport is successively controlled by three upstream modules of signal reception, initial signal processing, and Rho GTPase regulation. Our simulations indicated that an isotropic cell is polarized in response to a graded input signal. By applying a reversal gradient to a chemoattractant signal, lamellipod-specific molecules (i.e. PIP_3 and PI3K) disappear, first from the cell front, and then they redistribute at the opposite side, whereas functional molecules at the rear of the cell (i.e. PIP_2 and PTEN) act oppositely. In particular, the model cell exhibits a seesaw-like spatiotemporal pattern for the establishment of front and rear and interconversion, consistent with those related experimental observations. Increasing the switching frequency of the chemotactic gradient causes the cell to stay in a trapped state, further supporting the proposed dynamics of eukaryotic chemotaxis with the underlying cytoskeletal remodeling.

Introduction

Chemotaxis, or directed movement, of a eukaryotic cell toward the source of chemoattractant (hereafter shorted as CA), i.e. cAMP for *Dictyostelium* or fMLP for neutrophils, play an essential role in many pathophysiological processes (Parent 2004, Bagorda and Parent 2008). During embryogenesis, axons are steered by nerve growth factors to form the nervous system (Ruthel and Banker 2015). In immune responses, neutrophils are directed to the correct locations, and they kill the debris (Oliveira *et al* 2016). Chemotaxis is also central to wound healing and is implicated in tumor metastasis (Zimmermann 2017). For efficient movement, cells must sense the difference in CA concentration between its two ends, initiate the appropriate intracellular signaling cascade to mediate cytoskeletal remodeling and finally, form the well-defined *front* and *rear* regions (Devreotes and Janetopoulos 2003, Dalous *et al* 2008). At the front, the assembly of cytoskeletal actin propels the protrusion (Cai and Devreotes 2011). At the opposite side, actomyosin contracts and pulls up the rear (Parent 2004). Clearly, cells should be able to reverse their polarity for efficient targeting to the new source of CA (Gerisch and Keller 1981). That is, when a polarized cell is exposed to a sufficiently high CA gradient from the opposite direction, its initial front region could be reorganized transiently as the rear region and vice versa. Thus, understanding the dynamics of eukaryotic

chemotaxis is integral to elucidate biochemically induced cell movement.

In the past two decades, much progress, particularly with *Dictyostelium* and neutrophils, has been made by identifying additional components of the chemotactic pathways related to cytoskeletal remodeling (Ridley *et al* 2003, Parent 2004). The dynamic features of eukaryotic chemotaxis are a consequence of redistribution of intracellular signaling molecules; that is, the regions rich in Rac, Cdc42, PIP_3 are associated with actin branching and growth, while those rich in RhoA, PIP_2, and PTEN are correlated with myosin-II-induced contraction (Gardiner *et al* 2002, Kolsch *et al* 2008, Pramanik *et al* 2009). As the time scale of intracellular signaling responses is likely to be much shorter than those of gene expression and protein synthesis, spatiotemporal regulation of signaling pathways have become more interesting, especially when testing how cells effectively respond to spatiotemporally varied biochemical stimuli (Gardiner *et al* 2002). Experimentally, state-of-the-art techniques, such as microfabrication and *in vivo* imaging, have greatly facilitated quantitative analyses of intracellular signaling responses. For example, a microfluidic device can generate the precisely controlled gradient of extracellular CA (Ebrahimzadeh *et al* 2000, Meier *et al* 2011). Single-molecule imaging using fluorescent proteins enables highly sensitive quantification of cellular responses and cytoskeletal remodeling by simultaneously monitoring the spatiotemporal distribution of typical intracellular molecules (Ueda *et al* 2001, Sako *et al* 2012). Despite the different eukaryotic cell types used in those experiments (Weiner 2002, Dalous *et al* 2008), the dynamics of cellular chemotaxis are similar and can be summarized as follows. (1) *Adaptive*: the cells can sense a small difference in CA concentration between the front and rear regions over a wide range of mean concentrations (Parent 1999, Chen *et al* 2003). (2) *Rapid*: the cells generate the initial polarization in approximately 1–2 min (Weiner 2002). (3) *All-or-none*: the cells usually have one major pseudopod at a time (Dalous *et al* 2008). (4) *Tunable*: the cells continually adjust their polarized direction in response to new stimuli (Gerisch and Keller 1981, Dalous *et al* 2008). These four features are a prerequisite for a cell to undergo dynamic chemotaxis and should be included in a universal framework with the known signaling pathways.

Various mathematical models have been proposed to explore different mechanisms involved in intracellular signaling responses of chemotactic cells (Devreotes and Janetopoulos 2003, Iglesias and Devreotes 2008, Vanderlei *et al* 2011). The earliest turning-type model argues that the stable pattern of eukaryotic chemotaxis may arise if there is autocatalytic local production of a slow diffusive activator that also causes the production of a fast diffusive inhibitor (Meinhardt 1999). This model suggests symmetry breaks at the cellular scale with multiple activated regions; hence, the activation is not restricted to the front region. In addition, the model cell cannot change the direction of its polarity in response to a new stimulus, such that the entire system exhibits a 'lock-on' state. Several subsequent models have been developed based on a local excitation-global inhibition (LEGI) principle (Parent 1999, Ma *et al* 2004). In a basic LEGI model (Parent 1999), receptor occupancy triggers a fast, local excitatory signal and a slow, global inhibitory signal. At the cell front, the concentration of the activator is greater than the inhibitor and vice versa at the rear. Likewise, a balanced-inactivation model was also developed by considering two second messengers produced at equal rates (Levine *et al* 2006). The diffusion of one messenger, coupled with an inactivation scheme, ensures a switch-like response to external gradients over a wide range of mean concentrations. Lacking in these two models, however, are mechanisms of the role of actin-dependent pathways in regulating eukaryotic chemotaxis. To address these issues, an additional model was established based on a LEGI-biased excitable network hypothesis, where the LEGI scheme serves as an input to the downstream biochemical network that controls cytoskeletal activity (Xiong *et al* 2010). Unfortunately, these models do not account for stable polarity due to the difficulties in assigning polarity-specific components. Additionally, an antagonizing pathway model proposes that external stimuli activate two divergent pathways that mutually inhibit one another via interaction with the actin cytoskeleton (Onsum and Rao 2005), which can correctly localize and stabilize specific proteins to the respective front and rear regions of the cell. It also predicts that the cell slowly rotates its original pseudopods in response to a secondary reversal signal and simultaneously forms two pseudopods in response to a pair of stimuli, which does not agree with the experimental observations. Our previous work on the bidirectional molecular transport mechanism (Feng and Zhu 2014), in which the Rho GTPase-PIs feedback loops (PIs denote to PIP_3 and PIP_2 hereafter) are employed and the cell is treated as an intracellular and intra-membrane signal feedback system, has ignored the F-actin-independent pathway for simplicity. Finally, one more set of models was established by relying on the wave-pinning (WP) mechanism (Mori *et al* 2008, Walther *et al* 2012); namely, the evolution of a decelerating front is elicited by a transient and localized stimulus that becomes stationary due to overall mass conservation. Considering that the WP mechanism crucially depends on the exchange between active and inactive forms of signaling molecules with unequal diffusive rates, it is only suitable to describe the spatiotemporal evolution of Rho GTPases, not PIs, even though the latter could better represent the dynamics of cytoskeletal remodeling. Thus, universal models must be developed to unravel how signaling molecules form a polarized distribution to initiate the dynamic chemotaxis of a cell and then respond to a reversal CA stimulus.

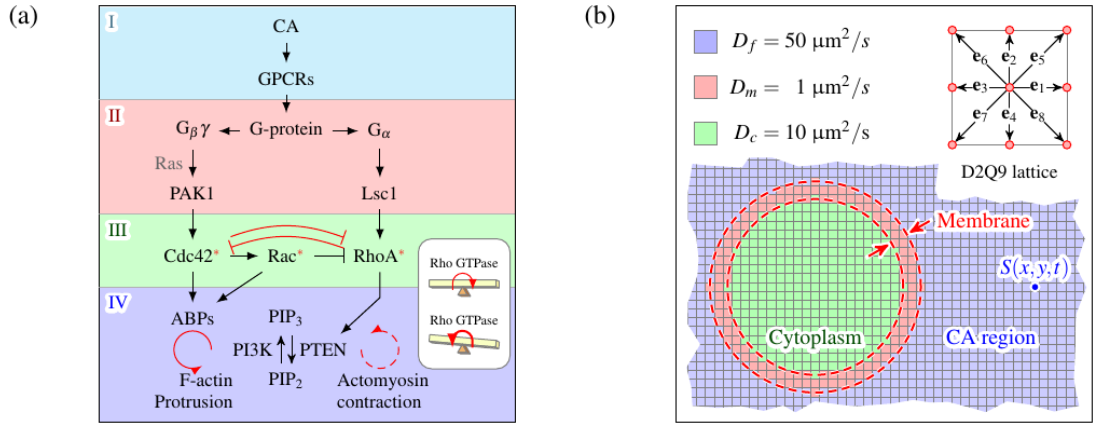

Figure 1. Model components and implantation. (*a*) Proposed signaling cascades. Here the cascades responsible for eukaryotic chemotaxis are reorganized into four modules. (I) Signal reception module: the cell senses the attractant molecules CA via GPCRs. (II) Initial signal processing module: G protein dissociates into G_α and $G_{\beta\gamma}$ subunits, which trigger a fast activation response and slower inhibition response. (III) Rho GTPase regulation module: spatial regulation of Rho GTPase members (Rac, Cdc42, and RhoA) is achieved by the localization of GEFs and the antagonistic effects between them. (IV) Bidirectional molecular transport module: spatial effects generated from Rho GTPase-PIs feedback loops control the bidirectional cytoskeletal remodeling. Curved solid and dashed arrows indicate the positive and negative feedback loops, respectively, and the insert illustrates the principle of our modeling. Here, a simple seesaw principle is used to demonstrate the core of the bidirectional molecular transport mechanism. That is, if the molecular transport toward one direction is enhanced compared to the opposite direction, the system would finally achieve an all-or-none response. Curved arrows in the insert illustrate the roles of upstreaming modules for controlling the positive direction of molecular transport. For initial polarization, the required directional cue is relative weak (depicted by fine arrows); for reversal polarization, the required directional cue from the opposite direction is strong (depicted by bold arrows). (*b*) Lattice–Boltzmann method for implementing the model. The geometry of the cell is modeled as a cycle structure. The whole computation domain is meshed by a D2Q9 lattice. The purple, red, and green lattices are specified as extracellular, membrane, and cytoplasm, respectively, and the molecular diffusion coefficients are specified as D_f, D_c, and D_m, respectively.

Here we present a multi-modular modeling framework for eukaryotic chemotaxis. Numerical simulations were designed to interpret a group of distinct but interrelated experimental observations, including initial polarization, reversal polarization, cell trapping, and cell mutation. Our modeling indicated that intracellular signaling responses with chemotactic pathways act as a bidirectional molecular transportation system controlled by a spatial gradient of active Rho GTPases that are transduced from the external signaling field. Physically, this prediction supports a surprisingly simple seesaw-like regulatory mechanism between the cell front and rear.

Biological backgrounds

Our modeling began by understanding that the primary components of chemotactic pathways among different kinds of eukaryotic cells are highly conserved, and signaling cascades are dominated by distinct mechanisms at different signaling layers (modules). As mentioned in our earlier work (Feng and Zhu 2014), four modules were applied, including signal reception (I), initial signal processing (II), small Rho GTPase regulation (III), and bidirectional molecular transport (IV). We propose a brief modeling strategy (figure 1(*a*)) and describe detailed descriptions of the molecular mechanisms involved in each module.

Signal reception

Cells sense the CA using transmembrane receptors (i.e. G protein-coupled receptors (GPCR)). The GPCRs are uniformly distributed along the plasma membrane (Parent 1999, Ridley *et al* 2003), which serves as an important regulator for cells to accurately sense the change in extracellular gradients.

Initial signal processing

The cascades between heterotrimeric G proteins (α, β, and γ) and F-actin independent signaling provide the initial amplification of sensed extracellular signals and adaptation mechanisms (Parent 2004, Stephens *et al* 2008). Upon CA binding to GPCRs, GTP can be exchanged for GDP on G_α subunits, leading to the dissociation of the G protein into G_α and $G_{\beta\gamma}$ subunits (Onsum and Rao 2005). The released $G_{\beta\gamma}$ subunits then stimulate a membrane-bound pool of PI3K in a Ras-dependent manner, while the G_α subunit is required for terminating $G_{\beta\gamma}$ activity (Sasaki *et al* 2007, Van Haastert and Devreotes 2004). The total amounts of G_α and $G_{\beta\gamma}$ are exactly the same, an essential requirement for achieving perfect adaptation.

Small Rho GTPase regulation

Rho-family small GTPases serve as central hubs in transducing signals from extracellular CA to the actin cytoskeleton (Raftopoulou and Hall 2004). The Rho GTPases are switch-like proteins that are cycled between active membrane-bound (GTP) forms and inactive cytosolic (GDP) forms (Raftopoulou and Hall 2004, Jilkine *et al* 2007). Activation of Rho GTPase is mediated by guanine exchange factors (GEFs) and inactivated by GTPase activating proteins (GAPs), while translocation of Rho GTPase from the membrane to cytosol is regulated by GDP dissociation inhibitors

Table 1. Parameter estimates relevant to four modules of modeling.

Parameter	Description	Value	Sources
D_f, D_c, D_m	Diffusion coefficients for extracellular, cytosolic, membrane species	50, 10, 1 $\mu m^2\ s^{-1}$	Korlach *et al* (1999) and Arrio-Dupont *et al* (2000)
K	Diminution rate of CA	1 s^{-1}	Postma *et al* (2001)
GR	Total number of GPCR	80 000	Ueda *et al* (2001) and Rappel and Levine (2008)
k_-	Dissociation rate	1 s^{-1}	Janssens and Van Haastert (1987) and Rappel and Levine (2008)
k_+	Association rate	30 $nM^{-1}\ s^{-1}$	Janssens and Van Haastert (1987) and Rappel and Levine (2008)
δ_A, δ_I	Diminution rates of activator, inhibitor	0.2, 0.2 s^{-1}	Levine *et al* (2006)
k_{AI}	Inactivation rate between activator and inhibitor	100 $\mu m\ (s \cdot molecule)^{-1}$	Levine *et al* (2006)
k_S	Production rate of activator and inhibitor	1, 1 s^{-1}	Levine *et al* (2006)
k_I	Association rate of inhibitor	3 $nM^{-1}\ s^{-1}$	Levine *et al* (2006)
R_{tot}, C_{tot}, ρ_{tot}	Total levels of Rac, Cdc42, RhoA	7.5, 3, 3 μM	Michaelson *et al* (2001) and Jilkine *et al* (2007)
R_b, C_b, ρ_b	Typical basal levels of active Rac, Cdc42, RhoA	3, 2.4, 1.25 μM	Maree *et al* (2006) and Maree *et al* (2012)
δ_R, δ_C, δ_ρ	Basal decay rates of active Rac, Cdc42, RhoA	1, 1, 1 s^{-1}	Zhang and Zheng (1998), Jilkine *et al* (2007) and Maree *et al* (2012)
I_R, I_C, I_ρ	Baseline activation rates of Rac, Cdc42, RhoA	0.4, 0.8, 0.4 s^{-1}	Maree *et al* (2006)
β, τ	Ecific GEF-dependent Cdc42, RhoA activation rates	3, 3 s^{-1}	Sakumura *et al* (2005)
α	Cdc42-dependent Rac activation rate	1 $\mu m\ (s \cdot molecule)^{-1}$	Otsuji *et al* (2007)
ε	Cdc42 and RhoA inactivation rate	1 $\mu m\ (s \cdot molecule)^{-1}$	Otsuji *et al* (2007)
γ	RhoA-dependent Rac inactivation rate	1 $\mu m\ (s \cdot molecule)^{-1}$	Otsuji *et al* (2007)
P_{2b}, P_{3b}	Basal levels of PIP2, PIP3	10, 0.45 μM	Ma *et al* (2004) and Maree *et al* (2012)
K_M^{PI3K}, K_M^{PTEN}	PIP3 and PIP2 level for half-max PI3K, PTEN feedback	8, 8 μM	Estimated
k_{cat}^{PI3K}, k_{cat}^{PTEN}	Enzymatic rates per active PI3K, PTEN	4, 4 s^{-1}	Estimated
R_{max}, ρ_{max}	Activity constants of Rac, RhoA	4, 1 μM	Estimated

(GDIs) (Raftopoulou and Hall 2004, Holmes *et al* 2012). Besides the self-regulation of each Rho-family member, there is considerable cross-talk between different members of the Rho-family (Jilkine *et al* 2007). Cdc42 is considered to serve as the upstream signal of Rac, while RhoA has mutual inhibitory interactions with Cdc42 and Rac (Gambardella and Vermeren 2013). The CA-induced spatial regulation of Rho GTPase could be initiated by G_α and $G_{\beta\gamma}$. For example, G_α activates specific Rho GEFs via PDZ-GEF/Lsc1 (Fenteany and Glogauer 2004), and $G_{\beta\gamma}$ binds to p21-activated kinase 1 (PAK1) and then activates Cdc42 via PAK-associated GEF (PIXα) (Gambardella and Vermeren 2013).

Bidirectional molecular transport

Once the gradient of active Rho-family GTPase is established, the spatial distributions generated by Rho GTPase and PIs tend to mediate positive/negative feedback loops (Weiner *et al* 2002, Charest and Firtel 2006), which drive bidirectional molecular transport. Intracellular transport of signaling molecules may orchestrate the localization of actin regulators and myosin activators, both of which are directly related to force generation mechanisms (Charest and Firtel 2006, Rottner and Stradal 2011).

Protrusive front region with highly active Cdc42/Rac

A role for small Rho GTPases in a self-organizing feedback loop of actin-PI3K-PIP_3 was proposed based on observations that latrunculin treatment and pharmacological inhibition of PI3K or Rho GTPases significantly blocks PIP_3 accumulation (Charest and Firtel 2006). Concretely, active Cdc42/Rac molecules interact with various actin-binding proteins (ABPs),

such as SCAR/WASP and Arp2/3 complex, which initiates F-actin polymerization (Parent 2004). During this process, PI3K is recruited from the cytosol to the membrane and catalyzes the phosphorylation of PIP_2 to produce PIP_3 (Stephens *et al* 2002, Van Haastert and Devreotes 2004). PIP_3 molecules then act as binding sites for various ABPs, which in turn promote F-actin polymerization and lead to the further membrane recruitment of PI3K and the repetition of the cycle (Sasaki *et al* 2007). The barbed ends of actin filaments proliferate by Arp2/3-mediated branching, extending until they reach the membrane and then exerting protrusion forces against the membrane (Rottner and Stradal 2011).

Rear region with highly active RhoA

Active RhoA molecules interact with phosphatidylinositol phosphatase (PTEN) (Li *et al* 2005), which is recruited from the cytosol to the membrane by PIP_2 (Sulis 2003). In its active form, PTEN antagonizes the action of PI3K by converting PIP_3 to PIP_2 (Weiner *et al* 2002, Sulis 2003, Billadeau 2008). Myosin-II is colocalized with PTEN, and its activity is regulated by myosin light-chain (MLC) phosphorylation, which is positively regulated by MLC kinase (MLCK) or Rho-associated kinase (ROCK) (Van Haastert and Devreotes 2004, Besser and Schwarz 2007). Consequently, actomyosin contracts and pulls up the rear.

Theoretical modeling

Consider that a cell is placed at a shallow CA filed, and only the contour membrane of the cell is assumed to sense the biochemical stimuli (figure 1(*b*)). By focusing on the spatiotemporal regulations of intracellular signal cascades, the structural elements inside the cell body are ignored, and the lamellipodium is treated as a cylindrical disk, with the cytosol as its interior and the cell membrane/cortex as its perimeter. There are different diffusive coefficients for molecular diffusion at extracellular regimes, the cytoplasm, and membranes, given as $D_f = 50$, $D_c = 10$, and $D_m = 1\ \mu m^2 \cdot s^{-1}$, respectively (table 1). Basic equations, derived from the above biochemical scheme (figure 1(*a*)), consist of a set of coupled partial differential equations (PDEs) that describe the reaction kinetics, cross-talk, diffusivity, and communication between the intermediate products. The translocation behaviors of those signaling molecules between the membrane and the cytosol are modeled in distinct ways. Proteins such as PI3K, PTEN, PAK1, and Lsc1, with limited amounts, are treated by a stochastic kinetics approach. In view of fast diffusion and a sufficient amount, the inactive cytosolic or GDP forms of Rho GTPase are assumed to be uniformly distributed in the cytosol and then calculated by the conservation law.

Basic equations

In this subsection, the equations and parameters are summarized for our modeling. Implementation decisions and simplifying assumptions are also discussed.

Signal reception

Diffusion and diminution of CA molecules were modeled by the reaction-diffusion equation, with corresponding initial and boundary conditions,

$$\frac{\partial S}{\partial t} = D_f \nabla^2 S - KS, \tag{1a}$$

$$\begin{aligned} &S(x,y,t) = S_0, \quad \text{for } x \in [x_1,x_2], y \in [y_1,y_2], \\ &S(x,y,0) = 0, \quad \text{for } x \notin [x_1,x_2], y \notin [x_1,y_2], \\ &S(X,Y,t) = 0, \end{aligned} \tag{1b}$$

where S, D_f, and K are the concentration, diffusive coefficient, and diminution rate of CA molecules, respectively. $x \in [x_1, x_2]$ and $y \in [y_1, y_2]$ define the domain of the point source, where the concentration of CA equals S_0. X and Y represent the boundary of the CA field. The binding kinetics of the CA molecules (as ligands) to the GPCRs (as receptors) are described by the following reaction equation,

$$R + L \underset{k_-}{\overset{k_+}{\rightleftarrows}} RL \tag{2}$$

where R, L, RL, k_+ and k_- represent receptor, ligand, complex, association rate, and dissociation rate, respectively.

Initial signal processing

The input CA signals need to be further translated into an intracellular asymmetry of signaling molecules. Here, we used a balance-inactivation mechanism to mimic this process (Levine *et al* 2006). The original mechanism proposed previously involves three interacting steps. First, the local level of receptor occupancy ($[RL]$) drives the production of a membrane-bound species A and a cytosolic species I at equal rates, k_s. Second, the cytosolic species diffuses inside the cell and attaches to the membrane at a rate k_I, where the membrane-anchored species I is denoted as I_m for our modeling. Finally, both species A and I_m inactivate each other with a rate k_i, and also A and I_m spontaneously degrade at the rates δ_A and δ_I respectively, which was used to mimic their biologic antagonism. The evolution dynamics of A, I and I_m are described as follows:

$$\frac{\partial A}{\partial t} = D_m \nabla^2 A + k_S[RL] - \delta_A A - k_i A I_m, \tag{3a}$$

$$\frac{\partial I_m}{\partial t} = D_m \nabla^2 I_m + k_I I - \delta_I I_m - k_i A I_m, \tag{3b}$$

$$\frac{\partial I}{\partial t} = D_c \nabla^2 I, \tag{3c}$$

with a boundary condition,

$$D_c \frac{\partial I}{\partial n} = k_S[RL] - k_I I. \tag{3d}$$

Upon the original balance-inactivation model, the abstract component activator A and inhibitor I can be identified as $G_{\beta\gamma}$ and G_α, respectively, even though

the mechanistic details responsible for their cross-talk are not explicitly explored. A and I_m may initiate the downstream Rho GTPase regulation module by interacting and/or incorporating with corresponding GEF of Rho GTPase via the intermediate messengers. In this model, we simply assumed that PAK1 and Lsc1 bind to the membrane at a rate proportional to the local density of A and I_m, respectively. The translocating behaviors of PAK1 and Lsc1 from the cytosol to the membrane are described by the binding reaction equation (equation (2)), where PAK1 and Lsc1 act as ligands, while A and I_m act as receptors. Because the numbers of PAK1 and Lsc1 (similar to PI3K and PTEN) are limited and their impacts on system behavior are significant, we identified them as effectors. Spatiotemporal evolution of cytosolic effectors obeys the following standard diffusion equation,

$$\frac{\partial E_c}{\partial t} = D_c \nabla^2 E_c, \tag{4a}$$

with a boundary condition for the outward pointing normal derivative of the cytosolic effectors,

$$D_c \frac{\partial E_c}{\partial n} = -k_+ S_m E_c + k_- M_c, \tag{4b}$$

where $E_c = E_{PAK1}$, E_{Lsc1}, E_{PI3K}, and E_{PTEN} represent the cytosolic concentrations of PIXα, Lsc1, PI3K, and PTEN, respectively, $M_c = M_{PAK1}$, M_{Lsc1}, M_{PI3K}, and M_{PTEN} define the membrane-bound concentrations of PAK1, Lsc1, PI3K, and PTEN, respectively, and S_m denotes the corresponding receptor concentration. Converting the concentration (in μM) into the site density of molecules (in μm^{-2}) is achieved by applying a factor, $\eta = 100\,mM^{-1}\ \mu m^{-2}$ (Gerisch and Keller 1981).

Small Rho GTPase regulation

We considered small Rho GTPases (Rac, Cdc42, RhoA) dynamics using a simplified model described previously, where mass conservation of various signaling components and diffusion-driven instability generates their polarized distribution (Otsuji *et al* 2007, Maree *et al* 2012). We assumed that each member of Rho GTPases was cycled between active membrane-bound forms and inactive cytosolic forms. The interactions among each member of Rho GTPases formed double negative feedback loops, as presented in the schematic of the Rho GTPases interactions in figure 1(*a*). The spatiotemporal evolution of active Rho GTPases is described as follows,

$$\frac{\partial G}{\partial t} = D_m \nabla^2 G + P_G\left(\frac{G_i}{G_{tot}}\right) - \omega_G G, \tag{5a}$$

where $G = R, C,$ and ρ represent the active (membrane-bound) forms of Rac, Cdc42, and RhoA, respectively. $G_{tot} = R_{tot}$, C_{tot}, and ρ_{tot} are the total concentrations of Rac, Cdc42, and RhoA, respectively. $G_i = R_i$, C_i, and ρ_i are the total concentrations of the respective inactive (cytosol) forms of Rac, Cdc42, and RhoA, calculated by the mass conservation law. P_G is the activation term and expressed as:

$$P_R = I_R + \alpha C,\ P_C = I_C + \beta E_C, \text{ and } P_\rho = I_\rho + \tau E_\rho. \tag{5b}$$

Here I_R, I_C, and I_ρ are the baseline activation rates. α sets the rate of Cdc42-enhanced Rac activation, β is the rate of GEF-mediated activation of Cdc42, and τ is the rate of GEF-mediated activation of RhoA. ω_G is the inactivation term and expressed as:

$$\omega_R = \delta_R + \gamma\rho,\ \omega_C = \delta_C + \varepsilon\rho, \text{ and } \omega_\rho = \delta_\rho + \varepsilon C. \tag{5c}$$

Here δ_R, δ_C, and δ_ρ are the GAP-mediated baseline inactivation rates. γ sets the rate of RhoA-mediated Rac inactivation, and ε is the mutual inactivation rate of Cdc42 and RhoA.

Bidirectional molecular transport

PIP_3 and PIP_2 are membrane lipids that play well-known regulatory roles in the actin-myosin cytoskeleton (Stephens *et al* 2008). PIP_3 provides binding sites for various ABPs to promote F-actin assembly and, thus, serves as the marker of the front of a polarized cell (Kolsch *et al* 2008). PIP_2 offers binding sites for myosin-II and, thus, serves as the marker of cell rear (Cai and Devreotes 2011). The spatiotemporal regulation of PIP_3 (P_3) and PIP_2 (P_2) forms the core of the bidirectional molecular transport mechanism, which is described by the following equations.

$$\begin{aligned}\frac{\partial P_3}{\partial t} =& D_m \nabla^2 P_3 + k_{cat}^{PI3K}\left(\frac{M_{PI3K} P_2 \widetilde{R}}{K_M^{PI3K} + P_2}\right) \\ & - k_{cat}^{PTEN}\left(\frac{M_{PTEN} P_3 \widetilde{\rho}}{K_M^{PTEN} + P_3}\right),\end{aligned} \tag{6a}$$

$$\begin{aligned}\frac{\partial P_2}{\partial t} =& D_m \nabla^2 P_2 + k_{cat}^{PTEN}\left(\frac{M_{PTEN} P_3 \widetilde{\rho}}{K_M^{PTEN} + P_3}\right) \\ & - k_{cat}^{PI3K}\left(\frac{M_{PI3K} P_2 \widetilde{R}}{K_M^{PI3K} + P_2}\right).\end{aligned} \tag{6b}$$

Here

$$\widetilde{R} = \min\left(\frac{R}{R_{max}}, 1\right), \quad \widetilde{\rho} = \min\left(\frac{\rho}{\rho_{max}}, 1\right).$$

In equation (6*a*), the first term on the right-hand side accounts for PIP_3 diffusion, the second represents PIP_3 production due to membrane-bound PI3K (M_{PI3K}) acting on PIP_2, and the third accounts for PIP_3 diminution due to membrane-bound PTEN (M_{PTEN}) acting on PIP_3. The value of k_{cat}^{PI3K} (k_{cat}^{PTEN}) is the maximum enzymatic rate per active PI3K (PTEN) molecule. K_M^{PI3K} (K_M^{PTEN}) is the typical level of PIP_3 (PIP_2) that gives half-maximum feedback via membrane-bound PI3K (PTEN). $\tilde{R}$ ($\tilde{\rho}$) is a normalized factor that defines the effect of Rac (Rho) activity on the activation of PI3K (PTEN). R_{max} (ρ_{max}) acts as a constant for Rac (RhoA) activity. If $\tilde{R}$ ($\tilde{\rho}$) is greater than R_{max} (ρ_{max}), the activity of Rac (RhoA) is no

longer a limiting factor for PI3K (PTEN) activation, and then $\widetilde{R}(\widetilde{\rho})$ equals unity.

Equation (6*b*) describes PIP_2 dynamics. Similarly, the first term on the right accounts for PIP_2 diffusion, the second represents the production of PIP_2 from PIP_3 via membrane-bound PTEN, and the third accounts for the reduction of PIP_2 into PIP_3 via membrane-bound PI3K. The total amounts of PIP_3 and PIP_2 remain constant over time. PI3K and PTEN act as key regulatory proteins of PIP_3/PIP_2 conversation, and both could translocate between the membrane and the cytosol by interacting with PIP_3 and PIP_2, respectively. While the active form feeds back onto its own production through cooperative binding, such a membrane-cytosol exchange cycle introduces the strongest feedback loop into the system.

Numerical methods

Numerical simulations were conducted with our previous work (Feng and Zhu 2014). Briefly, equations (1)–(6) were solved using the Lattice–Boltzmann method (LBM) within a static cell perimeter, in which a simple Monte–Carlo method was embedded to treat those stochastic source terms. The LBM approach is an auxiliary construct that possesses well-known computational advantages by using the fixed Cartesian meshes and straightforward implementation of boundary numerical schemes, allowing a smooth interpolation between the interior and exterior of the cell. The cell is placed in a regular grid containing 100×250 grid points and a grid spacing of 0.2 μm. Cell diameter is chosen to be 10 μm. A time step of 0.0025 s was used to solve the diffusion-reaction equation and implement the Monte–Carlo method. Initially, the concentrations of all signaling molecules were uniform in the interior of a circular domain, representing an unstimulated resting cell. All diffusible molecules satisfied the no-flux boundary conditions at the cell edge.

Results

Basic features of cell polarization

To assess whether the model represents basic experimental observations, we ran the full model (equations (1)–(6)) with biologically based parameter sets (table 1). The spatial positions of various molecules on the membrane were presented using a single variable θ, an angle varied between 0 and 2π. To eliminate the effect of the initial condition, the model cell underwent self-evolution in the absence of external stimuli to achieve a resting steady state (*data not shown*). To replicate point source-induced chemotaxis, the model cell was first simulated with a graded field formed by a CA point source 10 μm away from the cell for 200 s, followed by instantaneously switching the same point source to the opposite side at the location 5 μm away from the cell at $t = 200$ s for an additional 300 s thereafter. Except for the graded external stimulus, no front or rear regions of the cell were defined prior to the simulations. The spatiotemporal distributions of the integral molecule are shown in figure 2.

Initial graded stimulus period

After the initial introduction of the CA point source, the diffusion of CA molecules creates a concentration gradient around the cell perimeter (figure 2(*a*)). This steady-state CA field is established relatively fast, in less than 5 s, with an average concentration of approximately 1 nM and a gradient of 14.3×10^{-2} nM μm^{-1}. As a result of the high and fast dissociation rate of this binding event, the extracellular gradient of CA ligands is spatially mirrored by the graded occupancy of GPCRs (figure 2(*b*), *blue line*). The asymmetry in GPCR occupancy is spatially amplified by the fast signal processing process. The nascent, uniform front and rear regions are now marked by the accumulated $G_{\beta\gamma}$ and G_α, respectively (figure S1(*a*) and (*b*) (stacks.iop.org/PhysBio/15/056004/mmedia)), with no significant functional difference. The accumulation of $G_{\beta\gamma}$ and G_α introduces a local perturbation in Rho GTPase regulation by downregulating PAK1 and Lsc1 (figure S1(*c*) and (*d*)), respectively. Together with the mutual inhibition effects between RhoA and Cdc42, the stimuli-biased distributions of Cdc42 and RhoA are established (figures 2(*c*) and (*d*)). The reciprocal localization of Cdc42 and RhoA, along with their complementary regulation effects on Rac, ensures that Rac becomes positively regulated at the front and negatively regulated at the rear. Thus, the Rac activity displays a steeper gradient (figure 2(*e*) and (*e*′)). Spatial separation of Rho GTPase members then act as a compass to direct cytoskeletal remodeling. In the regions of high Rac/Cdc42 activity, elevated Rac enhances PI3K activation and, in turn, promotes a local increase in PIP_3 concentration. Local recruitment of PI3K from the cytosol to the membrane through PIP_3 induces a local reduction of PIP_2, which increases the dissociation of membrane-bound PTEN. Therefore, a short range positive feedback loop (Rac $\rightarrow$ PI3K $\leftrightarrows$ PIP_3) is formed, enabling PI3K and PIP_3 to be localized at the front (figures 2(*f*) and (*h*)). In regions of high RhoA activity, the previously dissociated PTEN from the front rebinds with PIP_2. After being activated by RhoA, these PTEN molecules cause further diminution of PIP_3 to produce PIP_2, which in turn forms a long-range negative feedback loop (RhoA $\rightarrow$ PTEN $\leftrightarrows$ PIP_2) that enables PTEN and PIP_2 to be localized at the rear (figures 2(*g*) and (*i*)). Such diffusion-driven bidirectional molecular transport is guided by the established internal Rho GTPase gradient and achieves a steady state when the pool of cytosol PI3K is significantly depleted. As a result, the final distribution of PIP_3 achieves an all-or-none pattern, ensuring that only a single lamellipodia is maintained.

Reversal graded stimulus period

Following the introduction of reversal stimuli at $t = 200$ s, the redistributed patterns of different

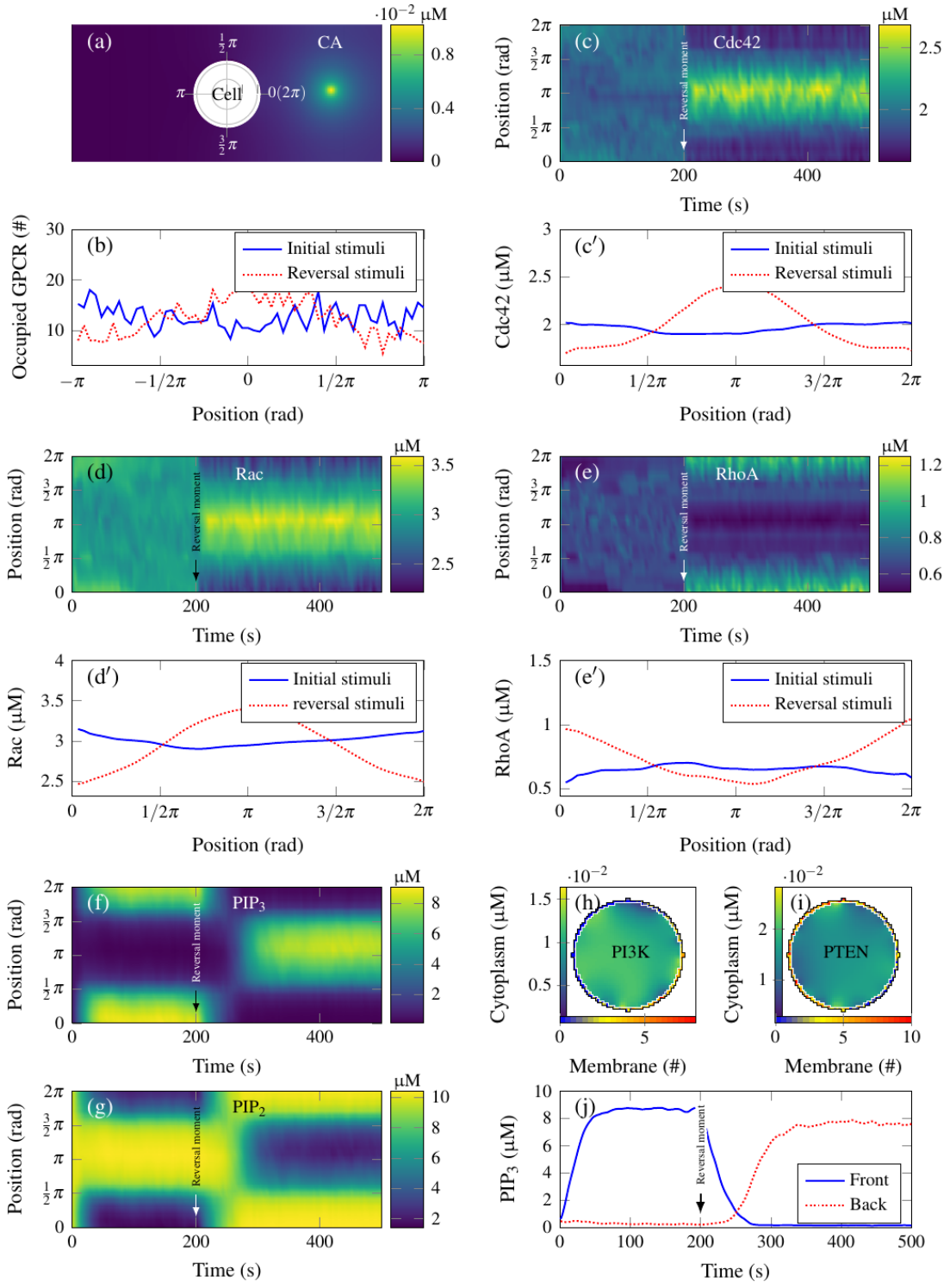

Figure 2. Basic features of polarization produced by WT model cell. (*a*) Spatial distribution of CA outside the cell. A micropipette containing constant CA concentration (considered as a point source) was initially placed at the middle right side of the cell. The diameter of the cell was 10 μm. (*b*) GPCR occupancy profiles at an initial stimulating time point ($t = 100$ s, *blue line*) and a reversal stimulating time point ($t = 300$ s, *red line*). (*c*)–(*g*) Simulations of spatiotemporal evolution of active Rho GTPases, that is, Cdc42 (*c*), Rac (*d*), and RhoA (*e*), and PIs, that is, PIP_3 (*f*) and PIP_2 (*g*), along the periphery of the model cell. The '0' angle is chosen to the time point toward the micropipette during the initial stimulus period. The spatial profiles of Rho GTPase (*c*′)–(*e*′) display shallow gradients (*blue lines*), in response to an initial stimulus, or steep gradients (*red lines*), in response to a stronger reversal gradient. PIP_3 and PIP_2 act as the markers of cell front and rear, respectively. Both display an all-or-none distribution pattern at the end of initial and reversal stimulus period. (*h*) and (*i*) Spatial distribution of PI3K (*h*) and PTEN (*i*) at $t = 100$ s, when the cell has already reached a well-polarized state. Initially, both PI3K and PTEN, as effectors, are set to be uniform in the cytosol with concentrations of 0.07 and 0.11 μM, respectively. Cytosolic distributions of the effectors generate fluctuations near the membrane region due to stochastic translocation behaviors. Local concentrations of membrane PI3K and PTEN are related to the local concentrations of cytosolic PIP_3 and PIP_2, respectively. (*j*) Concentration of PIP_3 as a function of time at the front (*blue line*) and the rear of the cell (*red line*). There is a clear delay period generated at the beginning of the reversal stimulus period (200–240 s), whereby the cell returns to an almost non-polarity state rather than generating two pseudopods at the same time.

regulatory proteins induced the cell to correctly repolarize according to the new stimuli (figures 2(*c*)–(*g*), $t = 500$ s). Specifically, the change in CA gradient was immediately sensed by the cell through the biased occupancy of GPCRs (figure 2(*b*), *red line*). Due to the introduction of balance-inactivation mechanism (equation (3)), the switch-like redistribution of $G_{\beta\gamma}$ and G_{α} constantly ensured the precise spatial control of PAK1 and Lsc1, such that the internal asymmetry in Rho GTPase was re-established along the new direction (figures 2(*c*)–(*e*)). The response was rapid: it reached a new steady state within 10 s. The spatial bipolar redistribution pattern of Rho GTPase was more significant. That is, active Rac and Cdc42 responses exhibited symmetric peaks facing the new point source (figures 2(*c*′) and (*d*′)), whereas active RhoA accumulated away from the source (figure 2(*e*′)). Such a redistribution of Rho GTPase greatly altered the local activation rate of PI3K and PTEN and, further, the direction of molecular transport. After approximately 120 s, PIs distribution achieved an all-or-none pattern, according to the new stimuli direction, as expected. There was also a significant delay in PIP_3 response to the reversal stimulus (figure 2(*j*), $t = 200$–240 s). In other words, the cell was predicted to return to an almost non-polarity state, but it was not predicted to spontaneously generate two major pseudopod. The specific molecular labels (i.e. PI3K, PIP_3) possibly disappeared first from the initial front and then reappeared at the opposite side because the inversion of cell polarity was initiated by a global inhibitor that turned down actin polymerization in the entire cell, followed by a fast-acting positive feedback loop raised to establish a new front (Dalous *et al* 2008). This global inhibitor was not necessarily required based on the current modeling. Rather, the spatiotemporal effect generated from Rho GTPase-PIs mediated feedback loops could well explain this phenomenon. Despite the fast redistribution of active Rho GTPase (figures 2(*c*)–(*e*)), the accumulation of PIP_3 at the initial front may still exist for a while (figures 2(*f*) and (*j*)), resulting in competition for cytosolic PI3K at two ends. Since the cytosolic PI3K could not effectively arrive at the new front side, the spatial effect of Rho GTPase-PIs mediated feedback loops was limited and no PIP_3 accumulation occurred there. After abolishing PIP_3 accumulation at the initial front, the competition for cytosolic PI3K between the two ends was won by the new front side. Henceforth, the spatial difference in Rho GTPase activity was continually amplified, which finally led to a full PIP_3 response at the new front side.

Effect of CA gradient steepness on cellular polarization

We tested the role of CA gradient steepness in eukaryotic chemotaxis. First, we quantified the effect of gradient steepness on the initial polarization by adjusting the distance between the point source and the cell. All other parameters remained the same. As shown in figure S2, four positions of the source point (*a*, *b*, *c*, and *d*, from far to near) were chosen, on which the formed steepest gradients were 2.8, 4.7, 7.9, and 14.3×10^{-2} nM μm^{-1}. mrespectively. Time courses of PIP_3 accumulation at the original cell front were compared, corresponding to each stimulus. As the applied stimulus gradient become steeper, the time required for the cell to achieve steady polarization became shorter and varied from 180 to 80 s. Meanwhile, the peak value of PIP_3 also increased from 6 to 9 μM. Msuggesting that the cell developed larger pseudopod in response to a steeper CA gradient. In addition, due to the balanced-inactivation mechanism introduced in the initial signal processing module, the modeled cell can respond to a 2% difference in CA concentration between the front and the rear of the cell (*data not shown*). Without a doubt, the required shallow CA gradient could be derived only if the cell was a distance of $3\lambda\left(\sqrt{\lambda = D_f/K}\right)$ from the source. By further adding a specific uniform CA field, the percentage variation of CA concentration across the cell could be simulated.

Next, we tested eukaryotic chemotaxis with different gradients of reversal stimulus. Similarly, three positions of CA point sources (*e*)–(*g*) were chosen (figure S2). From near to far, the formed reversal stimulus gradients were 43.7, 23.7 and 14.3×10^{-2} nM μm^{-1}, respectively. To reduce computational costs, those simulations were stated from the same planar polarized state. For each reversal stimulus condition, five successive snapshots of PIP_3 redistribution are presented in figure 3(*b*). In general, the steepness of the reversal gradient determined the dynamics of PIP_3 redistribution and further defined the cell reorientation. Particularly, in the case of the steepest reversal gradient (*point e*), PIP_3 first disappeared from the original front and then reappeared at the opposite side (figure 3(*b*), *top row*), suggesting that the cell reoriented itself in response to the new stimulus by generating an entirely new front. At mild steepness (*point f*), PIP_3 redistributed with slow rotation (figure 3(*b*), *middle*), implying that the cell preferred to make a *U*-turn to align to the new gradient. However, in the case of shallow steepness (*point g*), the cell was locked on the original distribution pattern of PIP_3 to a great extent (figure 3(*b*), *bottom row*), so that the cell could not reorient itself to the new stimulus.

Collectively, these simulations further illustrated the cooperativity of Rho GTPase-PIs mediated feedback loops. The appearance of PIP_3 accumulation resulted from the local strength of Rho GTPase-PIs mediated feedback loops, which indeed depended on both local Rac activity and PIP_3 concentration. In the initial cell polarization, Rac activity and PIP_3 concentration reached maximal values at the original front. Naturally, a steeper initial CA gradient induced a steeper intracellular Rho GTPase gradient, and accordingly, it evoked the spatial effect of Rho GTPase-

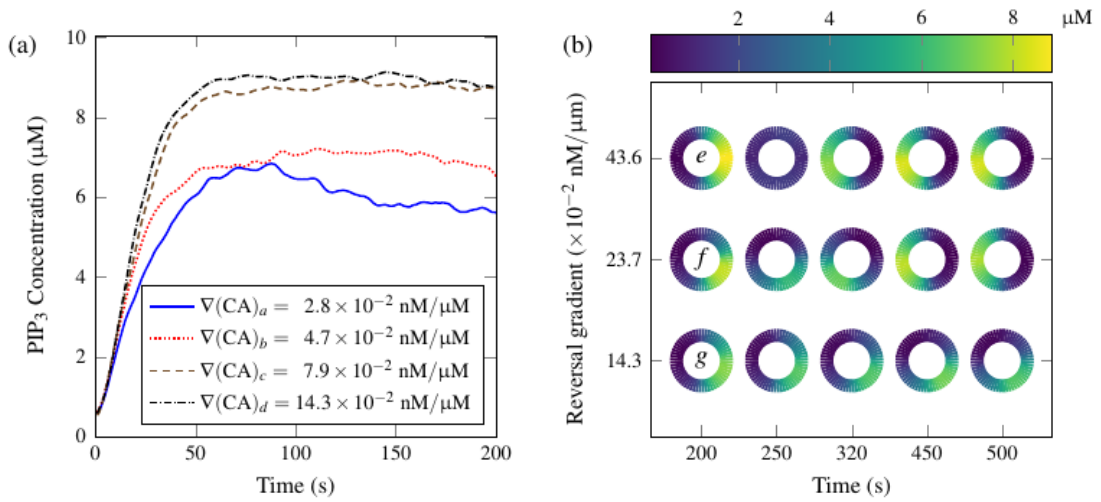

Figure 3. Effect of gradient steepness on cell polarization produced by a WT model cell. (*a*) Time course of PIP_3 accumulation at '0' angle as a function of different values of gradient steepness. As the initially applied gradient steepness decreased from 14.3 to 2.8×10^{-2} nM μm^{-1}, the time required to complete the initial polarization process increased from ~ 80 s to 180 s. (*b*) Five successive snapshots of PIP_3 spatial distribution upon different reversal gradients. The cell was initially polarized and exposed to the reversal stimulus at $t = 200$ s. Generally, the steepness of reversal CA gradient controls the dynamics of PIP_3 accumulation and further regulates the cell reorientation. (*b-top*) Upon the steepest reversal signal (43.7×10^{-2} nM μm^{-1}), PIP_3 first disappears from the front ($t = 250$s) and then reappears at the opposite side ($t = 320$ s), suggesting that the cell correctly repolarizes in the direction of the new gradient; (*b-middle*) with the less steep gradient of the reversal signal (23.7×10^{-1} nM μm^{-1}), PIP_3 was redistributed in a slowly rotating manner, suggesting that the cell prefers to make a *U*-turn to the new stimulus; (*b-bottom*) with the shallow reversal signal (14.3×10^{-1} nM μm^{-1}), PIP_3 accumulation froze at the front region during the entire reversal stimulus period; therefore, the cell cannot effectively reorient itself to the new stimulus.

PIs feedback loops in a rapid manner. In reversal polarization, the maximal value of PIP_3 concentration appeared at the original front, whereas the maximum local Rac activity occurred at the opposite side due to the fast dynamics. This mismatch in the distributions of active Rac and PIP_3 made the location of maximum feedback strength appear at the rear, near the original front, or at the original front, corresponding to the steepest, mildest, and shallowest stimulus, respectively.

Simulations with time-varied CA signals

To further validate this model, we also used a microfluidic function generator with double T-junction channels to alter the gradient direction of CA in a precise and time-dependent manner (Meier *et al* 2011). The most interesting finding was that a very fast switch frequency in the gradient direction led to a resting state for trapping the cells, compared to those at a stepwise reduction of gradient switching periods (from 200 s to 15 s). Our simulations indicated that, at a long period of $t = 200$ s, the PIP_3 response followed the varied gradients of the stimulus, indicating that the cell fully adjusts the polarity according to the respective gradient direction (figure 4(*a*)). At $t = 60$ s, the induced PIP_3 patches were less pronounced (figure 4(*b*)). Notably, the PIP_3 accumulation completely disappeared at the very rapid switching period of $t = 15$ s (figure 4(*c*)), suggesting that cytoskeletal remodeling ceased and the cell was chemotactically trapped in rapid switching. As an ideal case, a cell exposed to spatially uniform CA field was also simulated. Here, spontaneously appearing patches of PIP_3 could still be achieved (figure 4(*d*)), even though more time was required, compared with the gradient-induced case (figure 2(*f*)).

The underlying mechanism of this high frequency-dependent cell trap observation can also be well interpreted using the rational of our modeling. Basically, cell trapping is shaped by the balance between the efficient transport of intracellular molecules and the switch frequency of the external stimuli. If the switch frequency matches the rate of intracellular biochemical reorganization, the strength of the Rho GTPase-PIs mediated positive feedback loop becomes sufficiently strong to drive the bidirectional molecular transport. Here, the intracellular molecules display a successful shuttle run feature that is guided by temporally varied stimulus. However, if the switch frequency is much faster than the rate of intracellular molecular transport, the effect of external stimuli is limited to interrupt the spontaneous establishment of intracellular molecule patches, and no net molecular accumulation is achieved.

Chemotaxis dynamics of PTEN-mutated cells

Next, we analyzed how specific signaling molecules regulate the dynamics of eukaryotic chemotaxis. For example, the cytosolic concentration of PTEN molecules is either downregulated or upregulated for a cell exposed to the same initial or reversal stimulus (Sulis 2003, Subramanian *et al* 2007). Time courses of PIP_3 accumulation at the original front or rear regions are calculated in figures 5(a) and (b), respectively. For PTEN downregulation, a significant decrease in PTEN level ($(PTEN) = 0.03$ μM) induces a global high level of PIP_3 concentration (*blue lines*), implying

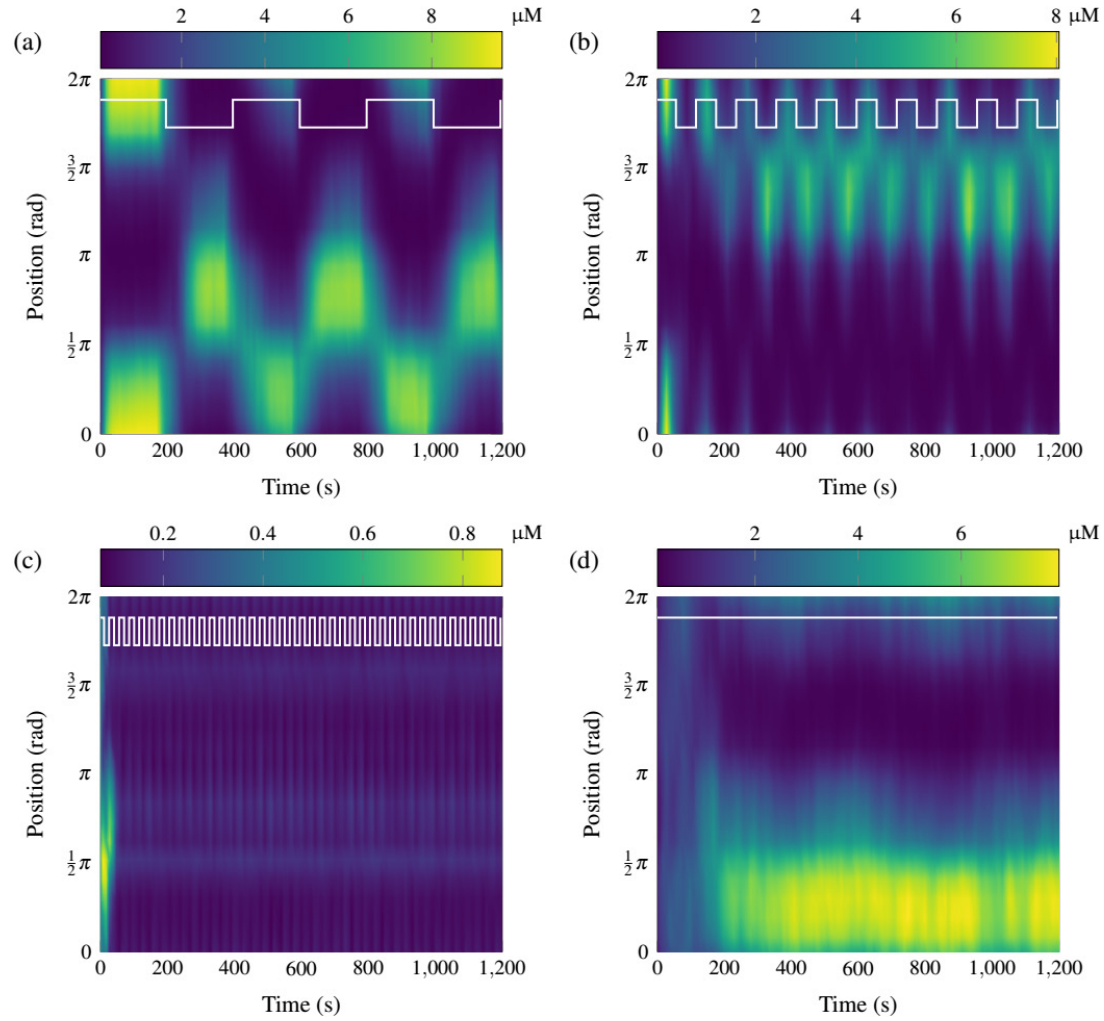

Figure 4. Elevated switching frequency of external gradient led to chemotactically trapped cells. (*a*) At a long exposure period of $t = 200$ s, cells read the direction of the signals and repeatedly reverses polarity. (*b*) At a relatively shorter period of $t = 60$ s, the appearance of PIP_3 patches still indicated the direction of stimulus but was less pronounced, suggesting that the cell has no time to develop polarity. (*c*) At the shortest period of $t = 15$ s, the cell completely lost PIP_3 patches corresponding to the chemotactically trapped cell state. (*d*) For the uniform stimulus condition as a control, the cell spontaneously developed PIP_3 patches. The *white line* in each panel indicates the temporally varied CA signal at the front of the cell.

that the cell could develop multiple, rather than single, pseudopod(s). A slight decrease ((PTEN) = 0.07 μM) reduced the delay in establishing new PIP_3 at the original rear side (*red lines*), compared with the 'wild-type' or WT cell at (PTEN) = 0.11 μM (*brown lines*). For PTEN upregulation, a slight increase ((PTEN) = 0.13 μM). Mresisted PIP_3 accumulation, as observed in the reduced PIP_3 concentration (*black lines*). Further increases in (PTEN) (=0.15 μM) completely abolished the establishment of reversal PIP_3 accumulation (*green lines*), suggesting a threshold value of PTEN concentration, above which the cell fails to develop reversal polarity.

This response pattern for a PTEN-varied cell upon initial CA stimulus can be deduced intuitively. Since the PTEN acts as an inhibitor toward the Rho GTPase-PIs mediated feedback loops, a PTEN-downregulated cell becomes easily excited, whereas a PTEN-upregulated cell has high inertia to prevent the excitation. Thus, those cellular behaviors, upon a reversal stimulus, could be better understood by analyzing typical time courses of the amount of cytosolic PI3K and PTEN (figure S2, derived from a WT cell). During the reversal stimulus period ($t = 200$–500 s), the strength of the positive feedback loop (Rac $\rightarrow$ PI3K $\leftrightarrows$ PIP_3) decreases at the original front and increases at the opposite side, while the negative feedback loop (RhoA $\rightarrow$ PTEN $\leftrightarrows$ PIP_2) acts oppositely. As a result, more membrane-bound PI3K molecules at the original front enter into the cytosol with a significant increase in cytosolic PI3K profile. In contrast, the PTEN profile demonstrates a significant reduction when more cytosolic PTEN molecules are recruited to the membrane. A critical time point at which the cell starts to rebuild its polarity was determined by the relative levels of cytosolic PI3K and PTEN. Naturally, it was more difficult for the PTEN-upregulated cell to achieve this critical point, showing a more significant delay phenomenon. Considering that the PTEN-downregulated cell failed to maintain only one major pseudopod upon initial and reversal polarization process, whereas the PTEN-upregulated cell had difficulty establishing initial polarity, it is

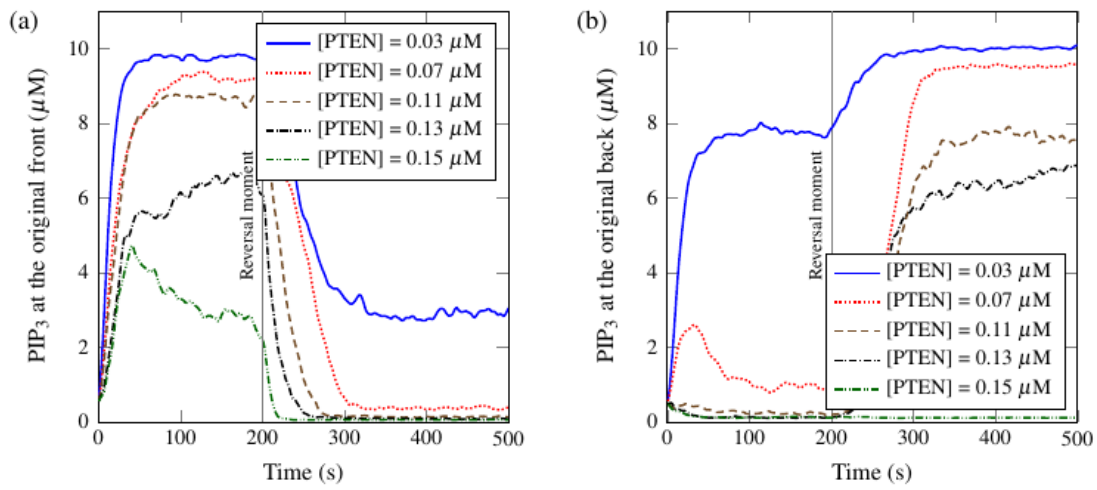

Figure 5. Responses of *PTEN*-mutant model cell to equalized stimulus. Time courses of PIP_3 accumulation at the original front (*a*) and original rear (*b*) that occur in various *PTEN* mutants. Compared with the WT cell ((*a*) and (*b*), *brown lines*), a significant decrease in PTEN expression ((PTEN) = 0.03 μM) resulted in a global high level of PIP_3 ((*a*) and (*b*), *blue lines*). With a slight decrease in PTEN ((PTEN) = 0.07 μM), the delay phenomenon in establishing the new front was reduced ((*a*), *red dotted line*), where a significant increase was present in the PIP_3 response at original rear at $t = 0$–30 s. This was attributed to a relative excess of PI3K that ensures the recruitment of PI3K at both cell ends. When more PTEN was transported backwards, the increase in the local strength of negative feedback loop impaired PIP3 response. A slight increase in PTEN expression ((PTEN) = 0.13 μM) resisted the establishment of PIP_3 accumulation, as reflected by the absolute level of PIP_3 concentration ((*a*) and (*b*), *black lines*). When PTEN was further increased ((PTEN) = 0.15 μM), the establishment of the reversal PIP_3 accumulation was completely abolished ((*a*) and (*b*), *green lines*), suggesting that a threshold for PTEN expression exists, above which cells fail to develop reversal polarity.

important for eukaryotic cells to maintain a proper level of PTEN. In addition, since the roles of PI3K and PTEN in regulating cell polarity are contrary (Parent 2002), decreasing PTEN or increasing PI3K has similar effect, and vice versa (*data not shown*).

Discussion

Considering theoretical modeling, our model can quantify the dynamics of rapid intracellular signaling responses in eukaryotic chemotaxis based on two aspects. First, in contrast to previous models treating intracellular signal cascades as a pure signal processing system relying on abstract inhibitory and activating components (Meinhardt 1999, Ma *et al* 2004), our model is centered on a molecular transport system and based on a realistic signaling network. Second, in contrast to most earlier models assuming that the interior of the cell is homogeneous (Onsum and Rao 2005), our model precisely accounts for cytosolic diffusion and the stochastic translocation behaviors of effector molecules, for example, the PIP_3 profiles. Although the simplification of cytosolic diffusion generates little effect on initial polarization of the cell, it brings up significant differences during reversal polarization. Here, a dramatically high value of the diffusion coefficient (i.e. $D_c = 30\ \mu m^2\ s^{-1}$) leads to a reduction of the delay and corresponds to the generation of pseudopods at two ends (figure S3). This is not surprised biophysically, because low diffusivity enables an effector molecule that has detached from the membrane to be trapped locally via reversible binding and unbinding events when the concentration of substrate molecules is sufficiently high. By contrast, an extremely high or even infinite diffusivity constant abolishes the trapping of those detached effector molecules. Thus, the introduction of realistic cytosolic diffusion of effector molecules is essential for a model to reflect biologically competitive effects between two signaling poles, which was not explicitly described in earlier theoretical studies.

Our modeling consists of four layered modules, and each module is dominated by a specific mechanism. This strategy is supported by a body of experimental evidence. For example, latrunculin-treated *Dictyostelium* cells adopt a spatial sensing mechanism that does not depend on the intact cytoskeleton (Janetopoulos *et al* 2004). Direct activation of endogenous Rac in HeLa cells enables the bypass of several upstream signaling molecules, and the graded activation triggers cellular polarization similar to that induced by exogenous CA gradients, implying that Rac activation serves as the start point in defining cytoskeletal remodeling (Holmes *et al* 2012). Moreover, various intermediate interactions exist among different modules (for example, PIP_3 provides binding sites for various GEFs, and in turn, it regulates Rho GTPase (Bagorda and Parent 2008). Accordingly, there should be an additional PIP_3 regulation module upstream of Rho GTPase. However, since this module only allows the cell to exceed the remodeling threshold without generating a shortboard effect on the entire system, this effect can be also included into the initial signaling processing module. Thus, we assumed a four layered module as a plausible scheme to embody the specific signal transduction cascades during eukaryotic chemotaxis (Parent 2004).

By comparing this model with existing experimental observations, we also gained several additional insights

into a system-level understanding of eukaryotic chemotaxis. One of the most important points is the conceptual role of an inhibitor. Inhibitors are required when modeling the signaling transduction of chemotaxis was initially postulated with the Turing-type model, in which the inhibitor is a rapidly diffusing protein, and its role is to induce diffusion-driven instability to achieve internal signal amplification (Meinhardt 1999). Following the popularity of the LEGI mechanism (Parent 1999, Ma *et al* 2004), it was widely accepted that a global inhibitor is mapped directly onto PTEN (Stephens *et al* 2002). Here, we proclaim that the inhibitor might be a group of molecules that provide negative effects at different stages of signal transduction, rather than a single molecule. For instance, G_α may act as an inhibitor in the initial signal processing module. According to the balance-inactivation mechanism, the inactivation effect between $G_{\beta\gamma}$ and G_α reasonably ensures the formation of a switch-like distribution or achieves the adaptation in response to uniform stimuli, even though experimental evidence to directly support this speculation is still lacking. By contrast, PTEN acts as inhibitor in the bidirectional molecular transport module. Its activity is regulated by RhoA, which, along with membrane and cytosol exchange through PIP_2, forms the core of the negative feedback loop that helps establish the polarity at the cell rear.

Our modeling also helps to elucidate when and how the cell develops polarity. Latrunculin-treated *Dictyostelium* cells generate bipolar localization of PIP_3 when simultaneously assigning two CA-filled micropipettes at the opposite sides of the cell, indicating that the cellular response at one side does not necessarily inhibit the response at the opposite side at the initial stage (Janetopoulos *et al* 2004, Van Haastert and Devreotes 2004). However, highly polarized cells cannot simultaneously respond at both the cell front and rear, mainly due to the spatiotemporal regulations of Rho GTPase-PIs mediated feedback loops in a seesaw-like pattern (figure 1(*a*), *insert*). At an initial CA gradient, the bipolar separation of small Rho GTPase members serves as a clear compass (as indicated by a rotation angle) to induce the rolling-over of the seesaw, resulting in an all-or-none distribution of internal molecules. To turn over the already-biased seesaw, the rotation angle from the opposite direction should be larger than the initial rotation angle, corresponding to a stronger reversal Rho GTPase compass signal. The biased seesaw also returns to a horizontal position for a non-polarity cell state. It should also be pointed out that both the processes of sensing a new target CA and rebuilding a polarized status for a cell yield different time scales. Generally, the former is much faster (in seconds) than the latter (in minutes) (Van Haastert and Devreotes 2004). To simplify the modeling in this work, we introduced the balance-inactivation mechanism to propose that the cell can always see the new target before it makes the reversal, U-turn, or lock-on decision based on a varied CA gradient.

While our simulations provide cellular responses that mirror most of the observed signaling responses in eukaryotic chemotaxis, several issues remain to be tested in the future. First, we simply used specific GPCR-mediated PI3K signaling pathways as the proxies for cytoskeletal remodeling, rather than modeling the entire signaling network. Actually, the coordinated polymerization and depolymerization of F-actin-based cytoskeleton are regulated by many other molecular mechanisms. For example, the former requires various ABPs, such as Arp2/3 and VASP (Stephens *et al* 2002, Rottner and Stradal 2011); the latter asks for, at least, the CA-mediated PLCβ/PI3Kγ/GSK3 signaling pathway. Adding these functional components to models could further the understanding of eukaryotic chemotaxis. Second, only biochemical factors are considered in the current work. In reality, mechanical cues such as matrix stiffness (Kuo *et al* 2012, Schaefer and Hordijk 2015) and shear flow (Dalous *et al* 2008, Wang *et al* 2014) are also crucial. When cells sense the mechanical factors using distinct mechanisms with stretch-activated ion channels or mechanosensitive cellular adhesive molecules, they are transduced into biochemical signals with common downstream signaling pathways (Vogel and Sheetz 2009). Thus, a systematic study of chemotaxis under mechanical stimuli would unveil new mechanisms of mechanotaxis by incorporating mechanical sensing modules. Finally, while our modeling attempted to capture the dynamic features of intracellular signaling responses, the model cell is still static. Qualitatively, if a cell moves toward the source, its internal signaling dynamics would be accelerated, since a steeper CA gradient should be met. Quantitatively, however, one may observe from the CA gradient profile (figure S2) that the influence of cellular motility on the intracellular signaling responses is negligible, as long as a cell is located farther than 3λ from the source. Nevertheless, our ongoing work is to incorporate a motility module into the current model, and this integrated model would be especially useful for unraveling the spatiotemporal regulation effects of internal signaling cascades upon the tunable cellular responses.

Conclusions

Rapid signaling responses are indispensable in implementing functions of a eukaryotic cell. In this work, we developed a 2D mathematical model for eukaryotic chemotaxis at an intermediate level of the molecular network. At least four key related features were validated from our modeling. First, active Rac/Cdc42, PIP_3, and PI3K were enriched at the front of the cell, whereas active RhoA, PIP_2, and PTEN were concentrated in the opposite rear side. Cell polarization was dynamically regulated by these core intracellular molecules and reached a steady state within 1–2 min. Second, there was a significant delay in generating new pseudopods when the cell responded

to a reversal stimulus, mainly due to competition for effector molecules (i.e. PI3K and PTEN) between two ends but not through an undiscovered global inhibitor. Third, the cell became trapped upon high-switching frequency of the direction of gradient stimulus. Finally, it was crucial to maintain the balance between the relative amounts of PI3K and PTEN molecules for proper initial and reversal polarization.

Acknowledgments

This work was supported by National Natural Science Foundation of China grants 31230027, 91539119, and 11502272, National Key Research and Development Program of China grant 2016YFA0501601, Strategic Priority Research Program grant XDB22040101, and Frontier Science Key Project grant QYZDJ-SSW-JSC018. The authors would like to acknowledge Professor Mian Long for his helpful suggestion.

ORCID iDs

Shi Liang Feng https://orcid.org/0000-0002-2637-0339

References

Arrio-Dupont M, Foucault G, Vacher M, Devaux P F and Cribier S 2000 Translational diffusion of globular proteins in the cytoplasm of cultured muscle cells *Biophys. J.* **78** 901–7

Bagorda A and Parent C A 2008 Eukaryotic chemotaxis at a glance *J. Cell Sci.* **121** 2621–4

Besser A and Schwarz U S 2007 Coupling biochemistry and mechanics in cell adhesion: a model for inhomogeneous stress fiber contraction *New J. Phys.* **9** 425

Billadeau D D 2008 PTEN gives neutrophils direction *Nat. Immunol.* **9** 716–8

Cai H and Devreotes P N 2011 Moving in the right direction: how eukaryotic cells migrate along chemical gradients *Semin. Cell Dev. Biol.* **22** 834–41

Charest P G and Firtel R A 2006 Feedback signaling controls leading-edge formation during chemotaxis *Curr. Opin. Genet. Dev.* **16** 339–47

Chen L, Janetopoulos C, Huang Y E, Iijima M, Borleis J and Devreotes P N 2003 Two phases of actin polymerization display different dependencies on PI(3,4,5)P3 accumulation and have unique roles during chemotaxis *Mol. Biol. Cell* **14** 5028–37

Dalous J, Burghardt E, Muller-Taubenberger A, Bruckert F, Gerisch G and Bretschneider T 2008 Reversal of cell polarity and actin-myosin cytoskeleton reorganization under mechanical and chemical stimulation *Biophys. J.* **94** 1063–74

Devreotes P and Janetopoulos C 2003 Eukaryotic chemotaxis: distinctions between directional sensing and polarization *J. Biol. Chem.* **278** 20445–8

Ebrahimzadeh P R, Hogfors C and Braide M 2000 Neutrophil chemotaxis in moving gradients of fMLP *J. Leukoc. Biol* **67** 651–61

Feng S and Zhu W 2014 Bidirectional molecular transport shapes cell polarization in a two-dimensional model of eukaryotic chemotaxis *J. Theor. Biol.* **363** 235–46

Fenteany G and Glogauer M 2004 Cytoskeletal remodeling in leukocyte function *Curr. Opin. Hematol.* **11** 15–24

Gambardella L and Vermeren S 2013 Molecular players in neutrophil chemotaxis--focus on PI3K and small GTPases *J. Leukocyte. Biol.* **94** 603–12

Gardiner E M, Pestonjamasp K N, Bohl B P, Chamberlain C, Hahn K M and Bokoch G M 2002 Spatial and temporal analysis of Rac activation during live neutrophil chemotaxis *Curr. Biol.* **12** 2029–34

Gerisch G and Keller H U 1981 Chemotactic reorientation of granulocytes stimulated with micropipettes containing fMet-Leu-Phe *J. Cell Sci.* **52** 1–10

Holmes W R, Lin B, Levchenko A and Edelstein-Keshet L 2012 Modelling cell polarization driven by synthetic spatially graded Rac activation *PLoS Comput. Bio.* **8** e1002366

Iglesias P A and Devreotes P N 2008 Navigating through models of chemotaxis *Curr. Opin. Cell Bio.* **20** 35–40

Janetopoulos C, Ma L, Devreotes P N and Iglesias P A 2004 Chemoattractant-induced phosphatidylinositol 3,4,5-trisphosphate accumulation is spatially amplified and adapts, independent of the actin cytoskeleton *Proc. Natl Acad. Sci. USA* **101** 8951–6

Janssens P M and Van Haastert P J 1987 Molecular basis of transmembrane signal transduction in Dictyostelium discoideum *Microbiol. Rev.* **51** 396–418

Jilkine A, Maree A F and Edelstein-Keshet L 2007 Mathematical model for spatial segregation of the Rho-family GTPases based on inhibitory crosstalk *Bull. Math. Biol.* **69** 1943–78

Kolsch V, Charest P G and Firtel R A 2008 The regulation of cell motility and chemotaxis by phospholipid signaling *J. Cell Sci.* **121** 551–9

Korlach J, Schwille P, Webb W W and Feigenson G W 1999 Characterization of lipid bilayer phases by confocal microscopy and fluorescence correlation spectroscopy *Proc. Natl Acad. Sci. USA* **96** 8461–6

Kuo C H, Xian J, Brenton J D, Franze K and Sivaniah E 2012 Complex stiffness gradient substrates for studying mechanotactic cell migration *Adv. Mater.* **24** 6059–64

Levine H, Kessler D A and Rappel W J 2006 Directional sensing in eukaryotic chemotaxis: a balanced inactivation model *Proc. Natl Acad. Sci. USA* **103** 9761–6

Li Z *et al* 2005 Regulation of PTEN by Rho small GTPases *Nat. Cell Biol.* **7** 399–404

Ma L, Janetopoulos C, Yang L, Devreotes P N and Iglesias P A 2004 Two complementary, local excitation, global inhibition mechanisms acting in parallel can explain the Chemoattractant-induced regulation of PI(3,4,5)P3 response in dictyostelium cells *Biophys. J.* **87** 3764–74

Maree A F, Jilkine A, Dawes A, Grieneisen V A and Edelstein-Keshet L 2006 Polarization and movement of keratocytes: a multiscale modelling approach *Bull. Math. Biol.* **68** 1169–211

Maree A F M, Grieneisen V A and Edelstein-Keshet L 2012 How cells integrate complex stimuli: the effect of feedback from phosphoinositides and cell shape on cell polarization and motility *PLoS Comput. Biol.* **8** e1002402

Meier B, Zielinski A, Weber C, Arcizet D, Youssef S, Franosch T, Radler J O and Heinrich D 2011 Chemotactic cell trapping in controlled alternating gradient fields *Proc. Natl Acad. Sci. USA* **108** 11417–22

Meinhardt H 1999 Orientation of chemotactic cells and growth cones: models and mechanisms *J. Cell Sci.* **112** 2867–74

Michaelson D, Silletti J, Murphy G, D'Eustachio P, Rush M and Philips M R 2001 Differential localization of Rho GTPases in live cells: regulation by hypervariable regions and RhoGDI binding *J. Cell Biol.* **152** 111–26

Mori Y, Jilkine A and Edelstein-Keshet L 2008 Wave-pinning and cell polarity from a bistable reaction-diffusion system *Biophys. J.* **94** 3684–97

Oliveira S D, Rosowski E E and Huttenlocher A 2016 Neutrophil migration in infection and wound repair: going forward in reverse *Nat. Rev. Immunol.* **16** 378–91

Onsum M and Rao C V 2005 A mathematical model for neutrophil gradient sensing and polarization *PLoS Comput. Biol.* **3** e36

Otsuji M, Ishihara S, Co C, Kaibuchi K, Mochizuki A and Kuroda S 2007 A mass conserved reaction–diffusion system captures properties of cell polarity *PLoS Comput. Biol.* **3** e108

Parent C A 1999 A Cell's Sense of Direction *Science* **284** 765–70

Parent C A 2002 PI 3-kinases and PTEN: how opposites chemoattract *Cell* **109** 541–4
Parent C A 2004 Making all the right moves: chemotaxis in neutrophils and Dictyostelium *Curr. Opin. Cell Biol.* **16** 4–13
Postma M and Haastert P J M V 2001 A diffusion–translocation model for gradient sensing by chemotactic cells *Biophys. J.* **81** 1314–23
Pramanik M K, Iijima M, Iwadate Y and Yumura S 2009 PTEN is a mechanosensing signal transducer for myosin II localization in Dictyostelium cells *Genes Cells* **14** 821–34
Raftopoulou M and Hall A 2004 Cell migration: Rho GTPases lead the way *Dev. Biol.* **265** 23–32
Rappel W J and Levine H 2008 Receptor noise and directional sensing in eukaryotic chemotaxis *Phys. Rev. Lett.* **100** 228101
Ridley A J, Schwartz M A, Burridge K, Firtel R A, Ginsberg M H, Borisy G, Parsons J T and Horwitz A R 2003 Cell migration: integrating signals from front to back *Science* **302** 1704–9
Rottner K and Stradal T E 2011 Actin dynamics and turnover in cell motility *Curr. Opin. Cell Biol.* **23** 569–78
Ruthel G and Banker G 2015 Role of moving growth cone-like wave structures in the outgrowth of cultured hippocampal axons and dendrites *Dev. Neurobiol.* **39** 97–106
Sako Y, Hiroshima M, Pack C G, Okamoto K, Hibino K and Yamamoto A 2012 Live cell single-molecule detection in systems biology *Wiley Interdiscip Rev. Syst. Biol. Med.* **4** 183–92
Sakumura Y, Tsukada Y, Yamamoto N and Ishii S 2005 A molecular model for axon guidance based on cross talk between rho GTPases *Biophys. J.* **89** 812–22
Sasaki A T, Janetopoulos C, Lee S, Charest P G, Takeda K, Sundheimer L W, Meili R, Devreotes P N and Firtel R A 2007 G protein-independent Ras/PI3K/F-actin circuit regulates basic cell motility *J. Cell Biol.* **178** 185–91
Schaefer A and Hordijk P L 2015 Cell-stiffness-induced mechanosignaling—a key driver of leukocyte transendothelial migration *J. Cell Sci.* **128** 2221–30
Stephens L, Ellson C and Hawkins P 2002 Roles of PI3Ks in leukocyte chemotaxis and phagocytosis *Curr. Opin. Cell Biol.* **14** 203–13
Stephens L, Milne L and Hawkins P 2008 Moving towards a better understanding of chemotaxis *Curr. Biol.* **18** 485–94
Subramanian K K, Jia Y, Zhu D, Simms B T, Jo H, Hattori H, You J, Mizgerd J P and Luo H R 2007 Tumor suppressor PTEN is a physiologic suppressor of chemoattractant-mediated neutrophil functions *Blood* **109** 4028–37
Sulis M 2003 PTEN: from pathology to biology *Trends Cell Biol.* **13** 478–83
Ueda M, Sako Y, Tanaka T, Devreotes P and Yanagida T 2001 Single-molecule analysis of chemotactic signaling in Dictyostelium cells *Science* **294** 864–7
Van Haastert P J and Devreotes P N 2004 Chemotaxis: signaling the way forward *Nat. Rev. Mol. Cell Bio.* **5** 626–34
Vanderlei B, Feng J J and Edelstein-Keshet L 2011 A computational model of cell polarization and motility coupling mechanics and biochemistry *Multiscale Model. Sim.* **9** 1420–43
Vogel V and Sheetz M P 2009 Cell fate regulation by coupling mechanical cycles to biochemical signaling pathways *Curr. Opin. Cell Biol.* **21** 38–46
Walther G R, Maree A F, Edelstein-Keshet L and Grieneisen V A 2012 Deterministic versus stochastic cell polarisation through wave-pinning *Bull. Math. Biol.* **74** 2570–99
Wang J, Lu D, Mao D and Long M 2014 Mechanomics: an emerging field between biology and biomechanics *Protein Cell* **5** 518–31
Weiner O D 2002 Regulation of cell polarity during eukaryotic chemotaxis: the chemotactic compass *Curr. Opin. Cell Biol.* **14** 196–202
Weiner O D, Neilsen P O, Prestwich G D, Kirschner M W, Cantley L C and Bourne H R 2002 A PtdInsP(3)- and Rho GTPase-mediated positive feedback loop regulates neutrophil polarity *Nat. Cell Biol.* **4** 509–13
Xiong Y, Huang C H, Iglesias P A and Devreotes P N 2010 Cells navigate with a local-excitation, global-inhibition-biased excitable network *Proc. Natl Acad. Sci. USA* **107** 17079–86
Zhang B and Zheng Y 1998 Regulation of RhoA GTP hydrolysis by the GTPase-activating proteins p190, p50RhoGAP, Bcr, and 3BP-1 *Biochemistry* **37** 5249–57
Zimmermann A 2017 *Mechanisms of Invasion and Metastasis: Cell Migration and Chemotaxis* (Berlin: Springer)